

Formation of Silver Nanoparticles at the Air–Water Interface Mediated by a Monolayer of Functionalized Hyperbranched Molecules

Beth M. Rybak, Maryna Ornatska, Kathryn N. Bergman, Kirsten L. Genson, and Vladimir V. Tsukruk*

Department of Materials Science and Engineering, Iowa State University, Ames, Iowa 50011

Received September 15, 2005. In Final Form: November 11, 2005

Nanofibrillar micellar structures formed by the amphiphilic hyperbranched molecules within a Langmuir monolayer were utilized as matter for silver nanoparticle formation from the ion-containing water subphase. We observed that silver nanoparticles were formed within the multifunctional amphiphilic hyperbranched molecules. The diameter of nanoparticles varied from 2–4 nm and was controlled by the core dimensions and the interfibrillar free surface area. Furthermore, upon addition of potassium nitrate to the subphase, the Langmuir monolayer templated the nanoparticles' formation along the nanofibrillar structures. The suggested mechanism of nanoparticle formation involves the oxidation of primary amino groups by silver catalysis facilitated by "caging" of silver ions within surface areas dominated by multibranching cores. This system provides an example of a one-step process in which hyperbranched molecules with outer alkyl tails and compressed amine-hydroxyl cores mediated the formation of stable nanoparticles placed along/among/beneath the nanofibrillar micelles.

Introduction

Many areas of technology continue to place a high demand on the miniaturization of critical components of microelectronic devices such as optical, magnetic, and electrical sensors and actuators. Most miniaturization strategies call for a new generation of composite materials based on inorganic nanoparticles and self-assembled molecular structures.^{1–6} Inorganic nanoparticles exhibit a unique array of physical, optical, and electrical properties that present great interest for microelectronic applications ranging from biosensing and catalysis to optics and data storage.^{7,8}

Numerous studies of a wide variety of inorganic nanoparticles with discrete compositions and sizes indicate that their properties are strongly affected not only by size and shape but by their surface composition, specific spatial ordering, and interactions with surrounding media.⁹ Whereas much research work has gone into controlling nanoparticle formation in solutions using wet

chemical synthesis,^{10,11} surfactants,^{12,13} and polymer templates such as dendrimers^{14–16} and hyperbranched molecules,¹⁷ the directed assembly of stable nanoparticles produced via these routes on solid substrates and interfaces remains challenging. The shape and dimensions of the nanoparticles remain very sensitive to the fine details of organic templates, and controlling their growth and aggregation on the nanometer scale can be tricky. In their 1951 paper, Turkevich et al. described a synthetic method for colloidal gold prepared by boiling a mixture of dilute HAuCl₄ and sodium citrate.¹⁸ Since then, extensive research has uncovered a great arsenal of chemical methods of synthesis

* Corresponding author. E-mail: vladimir@iastate.edu.

- (1) Tang Z.; Kotov N. A.; Giersig M. *Science* **2002**, *297*, 237.
- (2) Aguirre, C. M.; Kaspar, T. R.; Radloff, C.; Halas, N. J. *Nano Lett.* **2003**, *3*, 1707.
- (3) Peng, S.; Manna, U.; Yang, W.; Wickham, J.; Scher, E.; Kadavanich, A.; Alivisatos, A. P. *Nature* **2000**, *404*, 59.
- (4) (a) Decher, G.; Schlenoff, J. B., Eds. *Multilayer Thin Films*; Wiley-VCH: Weinheim, Germany, 2003. (b) Zhao, M.; Sun, L.; Crooks, R. M. *J. Am. Chem. Soc.* **1998**, *120*, 4877. (c) Crooks, R. M.; Zhao, M.; Sun, L.; Chechik, V.; Yeung, L. K. *Acc. Chem. Res.* **2001**, *34*, 181.
- (5) Lieber, C. *Nano Lett.* **2002**, *2*, 81.
- (6) (a) Jiang, C.; Markutsya, S.; Pikus, Y.; Tsukruk, V. V. *Nat. Mater.* **2004**, *3*, 721. (b) Jiang, C.; Markutsya, S.; Tsukruk, V. V. *Langmuir* **2004**, *20*, 882. (c) Jiang, C.; Markutsya, S.; Shulha, H.; Tsukruk, V. V. *Adv. Mater.* **2005**, *17*, 1669. (d) Markutsya, S.; Jiang, C.; Pikus, Y.; Tsukruk, V. V. *Adv. Funct. Mater.* **2005**, *15*, 771. (e) Ko, H.; Jiang, C.; Tsukruk, V. V. *Chem. Mater.* **2005**, *17*, 5489. (f) Jiang, C.; Markutsya, S.; Shulha, H.; Tsukruk, V. V. *Adv. Mater.* **2005**, *17*, 1669.
- (7) (a) Fendler, J. H. *Adv. Mater.* **2002**, *14*, 1006. (b) Xia, Y.; Yang, P.; Sun, Y.; Wu, Y.; Mayers, B.; Gates, B.; Yin, Y.; Kim, F.; Yan, H. *Adv. Mater.* **2003**, *15*, 353. (c) Chen, J.; Herricks, T.; Geissler, M.; Xia, Y. *J. Am. Chem. Soc.* **2004**, *126*, 10854.
- (8) Jin, R.; Cao, Y. C.; Hao, E.; Metraux, G. S.; Schatz, G. C.; Mirkin, C. A. *Nature* **2003**, *425*, 487.
- (9) (a) Manna, L.; Wang, L. W.; Cingolani, R.; Alivisatos, A. P. *J. Phys. Chem. B* **2005**, *109*, 6183. (b) Liu, H.; Alivisatos, A. P. *Nano Lett.* **2004**, *4*, 2397. (c) Scher, E. C.; Manna, L.; Alivisatos, A. P. *Philos. Trans. R. Soc. London, Ser. A* **2003**, *361*, 241. (d) Puentes, V. F.; Zanchet, D.; Erdonmez, C. K.; Alivisatos, A. P. *J. Am. Chem. Soc.* **2002**, *124*, 12874. (e) Manna, L.; Milliron, D. J.; Meisel, A.; Scher, E. C.; Alivisatos, A. P. *Nat. Mater.* **2003**, *2*, 382. (f) Puentes, V. F.; Krishnan, K. M.; Alivisatos, A. P. *Science* **2001**, *291*, 2115.

- (10) Quinn, M.; Mills, G. J. *Phys. Chem.* **1994**, *98*, 9840.
- (11) Pillai, Z. S.; Kamat, P. V. *J. Phys. Chem. B* **2004**, *108*, 945.
- (12) (a) Remita, S.; Mostafavi, M.; Delcourt, M. O. *New J. Chem.* **1994**, *18*, 581. (b) Khanna, P. K.; Sabbarao, V. V. *S. Mater. Lett.* **2003**, *57*, 2242. (c) Chen, S.; Carroll, D. *J. Phys. Chem.* **2004**, *108*, 5500. (d) Lee, C.-L.; Wan, C.-C.; Wang, Y.-Y. *Adv. Funct. Mater.* **2001**, *11*, 344. (e) Liz-Mazán, L. M.; Lado-Touriño, I. *Langmuir* **1996**, *12*, 3585. (f) Zhang, D.; Qi, L.; Yang, J.; Ma, J.; Cheng, H.; Huang, L. *Chem. Mater.* **2004**, *16*, 872. (g) Songping, W.; Shuyuan, M. *Mater. Chem. Phys.* **2005**, *89*, 423. (h) Yu, D.; Yam, V. W.-W. *J. Chem. Soc.* **2004**, *126*, 13200.
- (13) (a) Tang, Z.; Wan, Y.; Sun, K.; Kotov, N. A. *Adv. Mater.* **2005**, *17*, 358. (b) Tang, Z.; Kotov, N. A. *Adv. Mater.* **2005**, *17*, 951.
- (14) Esumi, K. *Top. Curr. Chem.* **2003**, *227*, 31.
- (15) (a) Balogh, L.; Valluzzi, R.; Laverdure, K.; Gido, S.; Hagnauer, G.; Tomalia, D. J. *Nanopart. Res.* **1999**, *1*, 353. (b) He, J.-A.; Valluzzi, R.; Yang, K.; Dolukhanyan, T.; Sung, C.; Kumar, J.; Tripathy, S. K.; Samuelson, L.; Balough, L.; Tomalia, D. *Chem. Mater.* **1999**, *11*, 3268. (c) Garcia, M.; Baker, L.; Crooks, R. *Anal. Chem.* **1999**, *71*, 256. (d) Wang, R.; Yang, J.; Caducci, M.; Jiao, J.; Seraphin, S. *Angew. Chem., Int. Ed.* **2001**, *40*, 549. (e) Li, L.; Cao, X.; Yu, F.; Yao, Z.; Xie, Y. *J. Colloid Interface Sci.* **2003**, *261*, 366. (f) Kim, M.-K.; Jeon, Y.-M.; Jeon, W.; Kim, H.-J.; Hong, S.; Park, C. *Chem. Commun.* **2001**, *67*. (g) Wu, X. C.; (h) Bittner, A. M.; Kern, K. *J. Phys. Chem. B* **2005**, *109*, 230. (i) Sun, X.; Dong, S.; Wang, E. *Macromolecules* **2004**, *37*, 7105.
- (16) (a) Esumi, K.; Houdatsu, H.; Yoshimura, T. *Langmuir* **2004**, *20*, 2536. (b) Esumi, K.; Isono, R.; Yoshimura, T. *Langmuir* **2004**, *20*, 237. (c) Esumi, K.; Akiyama, S.; Yoshimura, T. *Langmuir* **2003**, *19*, 7679. (d) Hayakawa, K.; Yoshimura, T.; Esumi, K. *Langmuir* **2003**, *19*, 5517. (e) Esumi, K.; Suzuki, A.; Yamahira, A.; Torigoe, K. *Langmuir* **2000**, *16*, 2604. (f) Esumi, K.; Suzuki, A.; Aihara, N.; Usui, K.; Torigoe, K. *Langmuir* **1998**, *14*, 3157. (g) Esumi, K.; Hosoya, T.; Suzuki, A.; Torigoe, K. *J. Colloid Interface Sci.* **2000**, *226*, 346.
- (17) (a) Aymonier, C.; Schlotterbeck, U.; Antonietti, L.; Zacharias, P.; Thomann, R.; Tiller, J.; Mecking, S. *Chem. Commun.* **2002**, *24*, 3018. (b) Lu, H. W.; Liu, S. H.; Wang, X. L.; Qian, X. F.; Yin, J.; Zhu, Z. H. *Mater. Chem. Phys.* **2003**, *81*, 104. (c) Zou, J.; Shi, W.; Hong, X. *Composites: Part A* **2005**, *36*, 631. (d) Lu, H. W.; Liu, S. H.; Wang, X. L.; Qian, X. F.; Yin, J.; Zhu, Z. K. *Mater. Chem. Phys.* **2003**, *81*, 104. (e) Garamus, V. M.; Maksimova, T.; Richtering, W.; Aymonier, C.; Thomann, R.; Antonietti, L.; Mecking, S. *Macromolecules* **2004**, *37*, 7893.

various metal nanoparticles.¹⁹ Recently, synthetic polymers have been gaining greater attention as templates for inorganic–organic hybrid materials. Because of a combination of simultaneous reducing and stabilizing functions and their ability to be easily functionalized to obtain specific properties as well as ligand properties, copolymers with a proper combination of functionalized groups may provide an easy and cost-efficient way to form nanoparticles in a variety of shapes and sizes.

The use of surfactants and amphiphilic copolymers to capture metal nanoparticles on a Langmuir–Blodgett (LB) trough provides a unique environment in which particle growth is controlled both by physical confinement and chemical capping. LB deposition is a viable and proven technique for the fabrication of nanoparticle arrays on solid substrates with ordered organic monolayers serving as a template for adsorbing nanoparticles from the water subphase.^{20–22} Typically, the incorporation of metal ions into ordered monolayers composed of low-molar-weight amphiphilic molecules (e.g., fatty acids or block copolymers) occurs at the air–liquid interface in close proximity to the polar heads of amphiphilic molecules.²³ Mono- or multilayer films containing nanoparticles or ions are then fabricated, and specific reducing agents should be used after the monolayer or multilayer transfer to solid substrates. The use of reducing agents in the subphase has also been reported as an alternative routine.²⁴ In a few instances, the use of a strong oxidizing agent for the oxidation of the headgroup of the amphiphile was observed to cause the reduction of the ions in the subphase and thus the formation of the nanoparticles²⁵ and nanoribbons under the Langmuir monolayer.²⁶ However, in most cases these processes are time-consuming, contain multistep routines, require additional reducing agents, and, in the case of dendrimers, can be quite expensive for large-scale fabrication. In addition, a major issue is the wide distribution of dimensions and the scarce, inhomogeneous growth of metal nanostructures.

In the work reported herein, the unique spatial constraints created at the air–liquid interface by the nanofibrillar morphology of the functionalized amphiphilic hyperbranched molecules with a hydrophilic core and a hydrophobic shell were utilized to control the adsorption of silver ions from the water subphase. The multifunctional character of hyperbranched molecule with hydroxyl and amine groups in the hydrophilic polyester core combined with the hydrophobic alkyl shell was observed to

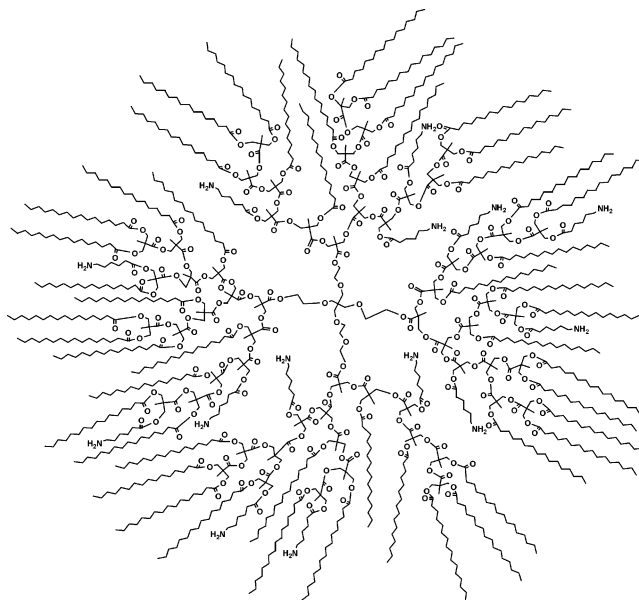


Figure 1. Idealized chemical structure of HBP.²⁸

provide the necessary balance in assisting silver ion adsorption from the water subphase. The formation of silver nanoparticles under/within the monolayer filled with nanofibrillar bundles of semispherical micelles from hyperbranched molecules²⁷ was observed to occur without the use of external reducing agents or a postdeposition treatment step. The one-step method demonstrated here that uses organized hyperbranched molecules at the air–liquid interface provides an effective and straightforward alternative to the multistep processes that have been reported to date. The approach suggested generates very uniform silver nanoparticles with a diameter of 2–4 nm and, under certain conditions, promotes their chainlike aggregation.

Experimental Section

Amphiphilic hyperbranched copolymer (HBP) was synthesized from commercially available hyperbranched polyester polyol Boltorn BH40 (Perstorp Inc.).²⁷ Amphiphilic HBP synthesized according to the procedure described earlier contains 50 hydrophobic palmitic (C₁₆) alkyl tails and 13 amine (–NH₂) and 1 to 2 hydroxyl-terminated polar branches as presented in the ideal chemical structure (Figure 1).²⁸ The ability of the HBP to form one-dimensional nanofibers at the air–water interface upon compression of Langmuir monolayers made it an attractive candidate for the formation of silver nanoparticles. The HBP molecules in the Langmuir monolayer were expected to capture silver ions from the AgNO₃ subphase because of the ligand interactions with primary amine groups presented and to further reduce silver ions to metal nanoparticles.

Silver nitrate (Fisher Scientific), potassium nitrate (Fisher Scientific), and sodium borohydride (Aldrich) were used as received. The synthesis and chemical structure of the amphiphilic HBP have been described in recent publications^{27–29} (Figure 1). The HBP was dissolved in chloroform (1 mg/mL), and deposition at the air–water interface was conducted using the known procedure.³⁰ A Riegel & Kirstein, GmbH (R&K-1), trough and a KSV Minitrough trough were used for LB monolayer fabrication and surface pressure–area

(18) Turkevich, J.; Stevenson, P. S.; Hillier, J. *Discuss. Faraday Soc.* **1951**, *11*, 58.

(19) (a) Masala, O.; Seshadri, R. *Annu. Rev. Mater. Res.* **2004**, *34*, 41. (b) Cushing, B. L.; Kolesnichenko, V. L.; O'Connor, C. J. *Chem. Rev.* **2004**, *104*, 3893. (c) Botha, S. S.; Brijoux, W.; Brinkmann, R.; Feyer, M.; Hofstadt, H.-W.; Kelashvili, G.; Kinge, S.; Matoussevitch, N.; Nagabhushana, K. S.; Wen, F. *Appl. Organomet. Chem.* **2004**, *18*, 566.

(20) Ulman, A. *An Introduction to Ultrathin Organic Films: From Langmuir–Blodgett to Self-Assembly*; Academic Press: Boston, 1991.

(21) (a) Elliot, D.; Furling, D.; Neil, G.; Grieser, F. *Colloids Surf., A* **1999**, *155*, 101. (b) Elliot, D.; Grieve, K.; Furlong, N.; Grieser, F. *Adv. Colloid Interface Sci.* **2001**, *91*, 113. (c) Erokhin, V.; Troitsky, V.; Erokhina, S.; Mascetti, G.; Nicolini, C. *Langmuir* **2002**, *18*, 3185. (d) Kapoor, S.; Lawless, D.; Kennepohl, P.; Meisel, D.; Serpone, N. *Langmuir* **1994**, *10*, 3018. (e) Ewins, C.; Stewart, B. *Thin Solid Films* **1996**, *284*, 49. (f) O'Driscoll, B.; Gentle, I. *Langmuir* **2002**, *18*, 6391. (g) Li, H.; Mao, G.; Simon Ng, K. *Thin Solid Films* **2000**, *358*, 62. (h) Lindén, D.; Peltonen, J.; Rosenbolm, J. *Langmuir* **1994**, *10*, 1592. (i) Samokhvalov, A.; Gurney, R. W.; Lahav, M.; Cohen, S.; Cohen, H.; Naaman, R. *J. Phys. Chem. B* **2003**, *107*, 4245. (j) Leloup, J.; Maire, P.; Ruau-del-Teixier, A.; Barraud, A. *Mol. Cryst. Liq. Cryst.* **1986**, *134*, 347. (k) Ravaine, S.; Fanucci, G. E.; Seip, C. T.; Adair, J. H.; Talham, D. R. *Langmuir* **1998**, *14*, 708. (l) Mansur, H. S.; Grieser, F.; Marychurch, M. S.; Biggs, S.; Urquhart, R. S. *J. Chem. Soc., Faraday Trans.* **1995**, *91*, 665.

(22) Tsukruk, V. V. *Prog. Polym. Sci.* **1997**, *22*, 247.

(23) Chung, A. J.; Rubner, M. F. *Langmuir* **2002**, *18*, 1176.

(24) Yi, K. C.; Hórvölgyi, Z.; Fendler, J. H. *J. Phys. Chem.* **1994**, *98*, 3872.

(25) Swami, A.; Selvannan, P. R.; Pasricha, R.; Sastry, M. *J. Phys. Chem. B* **2004**, *108*, 19269.

(26) Swami, A.; Kumar, A.; Selvakannan, P.; Mandal, S.; Pasricha, R.; Sastry, M. *Chem. Mater.* **2003**, *15*, 17.

(27) (a) Ornatka, M.; Bergman, K. N.; Rybak, B.; Peleshanko, S.; Tsukruk, V. V. *Angew. Chem.* **2004**, *116*, 5358. (b) Ornatka, M.; Peleshanko, S.; Rybak, B.; Holzmueller, J.; Tsukruk, V. V. *Adv. Mater.* **2004**, *16*, 2206.

(28) Ihre, H.; Johansson, M.; Malmstrom, E.; Hult, A. *Adv. Dendritic Macromol.* **1996**, *3*, 1.

(29) Ornatka, M.; Peleshanko, S.; Genson, K.; Rybak, B.; Bergman, K.; Tsukruk, V. J. *Am. Chem. Soc.* **2004**, *126*, 9675.

(30) (a) Blodgett, K. A. *J. Am. Chem. Soc.* **1935**, *57*, 1007; Blodgett, K. A. *Phys. Rev.* **1937**, *51*, 964. (b) Tsukruk, V. V.; Bliznyuk, V. N.; Hazel, J.; Visser, D.; Everson, M. P. *Langmuir* **1996**, *12*, 4840.

(π - A) isotherm collection. Subphase solutions contained 0.1–5 mM AgNO_3 and 22 mM KNO_3 dissolved in NanoPure water (resistivity > 18 M Ω cm). All monolayers were deposited at a surface pressure of 10 mN/m onto a polished silicon substrate with (100) orientation that had been cleaned prior to use with piranha solution as described elsewhere.^{31,32}

Tapping-mode atomic force microscopy (AFM) imaging was used in a light tapping mode to ensure that the polymer layer was not damaged during the scanning of the monolayers.³³ Dimension-3000 and Multimode (Digital Instruments) microscopes were utilized for these studies. Ultrasharp tips with radii below 15 nm were used for the imaging (typical spring constant 3 N/m and average drive frequency 75 kHz). The actual tip radius was determined before high-resolution scanning by imaging a gold nanoparticle standard sample using a known technique.³⁴ The typical size of an image obtained in this work was 0.5–10 μm .

For X-ray photoelectrospectroscopy (XPS) studies of LB monolayers, a Perkin-Elmer Multitechnique Chamber, model 5500, was used to determine the chemical composition of the thin films. The experimental error for the high-resolution spectra was ± 0.25 eV. The data were smoothed using a three-point smoothing function.

Grazing incidence X-ray diffraction (GIXD) synchrotron studies on Langmuir layers at the air–liquid interface were performed at the 6ID beamline at the Advanced Photon Source (APS) at Argonne National Laboratory.^{35,36} An in-depth description of the setup and experimental procedure is provided elsewhere.³⁷ A germanium monochromator was used to select the X-ray beam energy ($\lambda = 0.07653$ nm). A Phillips CM30 electron microscope with a LaB6 filament was operated at 300 kV and used to perform transmission electron microscope (TEM) studies of the monolayers deposited on silicon oxide and Formvar-covered TEM grids purchased from Ted Pella.

Results and Discussion

Surface Behavior. The effect of the presence of AgNO_3 in the subphase of a Langmuir monolayer of amphiphilic hyperbranched molecules was studied with π - A isotherms. As was observed, the HBP monolayer exhibited classic amphiphilic behavior on both water and aqueous AgNO_3 subphases (Figure 2). The limiting cross-sectional area of HBP did not change significantly in the presence of AgNO_3 in the subphase. When the concentration of AgNO_3 was increased (concentrations of 0.1, 1, and 5 mM were used), the only measurable change in the surface area per molecule (~ 1 nm²) occurred when a 5 mM AgNO_3 solution was used. We concluded that because of the molecular conformation of the HBP at the air–water interface the retaining of silver ions would occur under the large molecules and thus would not significantly affect the limiting cross-sectional area. Indeed, from geometrical considerations, the differences in magnitude between the lateral dimensions of the HBP molecule²⁸ (12 nm²) and that of the silver ion (0.08 nm²) indicate that changes in the overall surface areas will be insignificant if fewer than 5–10 ions are adsorbed. The initial molecular area at π - A isotherms (the takeoff molecular area) was also observed to change when the concentration of AgNO_3 in the subphase was greater

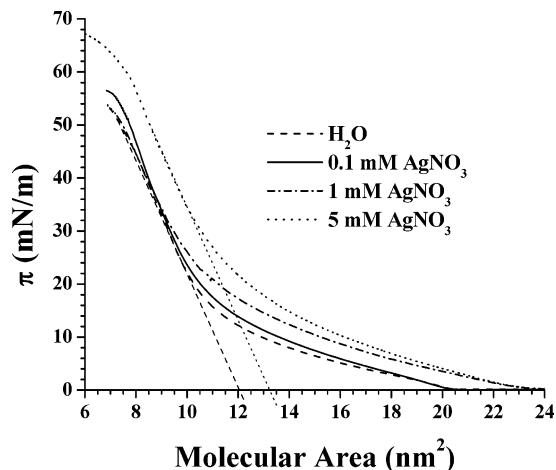


Figure 2. π - A isotherms of HBP on subphases with different aqueous AgNO_3 content. Straight lines are drawn to show the limiting cross-sectional area for two limiting cases only.

than 0.1 mM, with a magnitude of change of 3.3 nm². Therefore, the association of amino groups with an increased number of silver ions in the subphase could be attributed to the observed increase in the takeoff molecular area on the pressure isotherms at higher AgNO_3 concentrations. Similar results were previously reported for monolayers of low-molar-weight amphiphiles at the air–liquid interface when an increase in the takeoff molecular area was indicated in the presence of elevated concentrations of ions in the subphase. This effect was associated with complexing of the surfactant's polar headgroup with the ions in the subphase.²⁵

Another phenomenon observed was an increased stability afforded to the HBP by the presence of AgNO_3 in the subphase as indicated by the increased pressure of monolayer collapse (Figure 2). Monolayer collapse was observed to occur at a surface pressure of 68 mN/m when the concentration of AgNO_3 was 5 mM, which was in contrast to the 54 mN/m collapse pressure measured when the subphase was Nanopure water. Similar stabilization effects due to the presence of metal ions were reported previously for amphiphilic block copolymers.³⁸

LB Monolayers. The morphology of the silver-containing LB monolayer deposited on a silicon wafer was affected by the amount of AgNO_3 in the subphase. A series of experiments were conducted with concentrations of 0.1, 1, and 5 mM AgNO_3 . After 7 and 24 h on a subphase of 5 mM AgNO_3 , larger aggregates of nanoparticles up to 100 nm across were observed (Figure 3a and b). When the concentration decreased to 1 mM AgNO_3 , the nanoparticle size shifted to smaller values for both the 7 and 24 h experiments (Figure 3c and d). The histogram of nanoparticle heights under these conditions showed an average height of 2.6 ± 0.9 nm (Figure 4a). When the concentration of AgNO_3 was further decreased to 0.1 mM, the concentration of nanoparticles increased (Figure 3e and f). The average height of these nanoparticles was 2.5 ± 1 nm for the longest adsorption time (Figures 4b and 5b). Typical nanofibril morphology of the HBP monolayer was clearly visible for any deposition, but generally little correlation was observed between nanofibril structures and nanoparticle locations.

An HBP monolayer was also deposited onto a Formvar-covered TEM grid, after 7 h of exposure on a subphase of 0.1 mM AgNO_3 . The TEM image of this sample in Figure 5a shows a relatively low density of silver nanoparticles adsorbed under these conditions. A histogram of diameter distribution (Figure 5b) compiled from the TEM image revealed that the distribution of

(31) (a) Sidorenko, A.; Zhai, X. W.; Peleshanko, S.; Greco, A.; Shevchenko, V. V.; Tsukruk, V. V. *Langmuir* **2001**, *17*, 5924. (b) Peleshanko, S.; Gunawidjaja, R.; Jeong, J.; Shevchenko, V. V.; Tsukruk, V. V. *Langmuir* **2004**, *20*, 9423. (c) Genson, K. L.; Hoffman, J.; Teng, J.; Zubarev, E. R.; Vaknin, D.; Tsukruk, V. V. *Langmuir* **2004**, *20*, 9044. (d) Zhai, X.; Peleshanko, S.; Klimenko, N. S.; Genson, K. L.; Vortman, M. Ya.; Shevchenko, V. V.; Vaknin, D.; Tsukruk, V. V. *Macromolecules* **2003**, *36*, 3101.

(32) Tsukruk, V. V.; Bliznyuk, V. N. *Langmuir* **1998**, *14*, 446.

(33) Tsukruk, V. V. *Rubber Chem.* **1997**, *70*, 430.

(34) Tsukruk, V. V.; Reneker, D. H. *Polymer* **1995**, *36*, 1991.

(35) Larson, K.; Vaknin, D.; Vallavicencio, O.; McGrath, D.; Tsukruk, V. V. *J. Phys. Chem. B* **2002**, *106*, 7246.

(36) Larson, K.; Vaknin, D.; Vallavicencio, O.; McGrath, D.; Tsukruk, V. V. *J. Phys. Chem. B* **2002**, *106*, 11277.

(37) Vaknin, D. In *Methods of Materials Research*; Kaufmann, E. N., Abaschian, R., Barnes, P. A., Bocarsly, A. B., Chien, C. L., Doyle, B. L., Fultz, B., Leibowitz, L., Mason, T., Sanchez, J. M., Eds.; John Wiley & Sons: New York, 2001.

(38) Jeong, H.; Lee, B.-J.; Cho, W.; Ha, C.-S. *Polymer* **2000**, *41*, 5525.

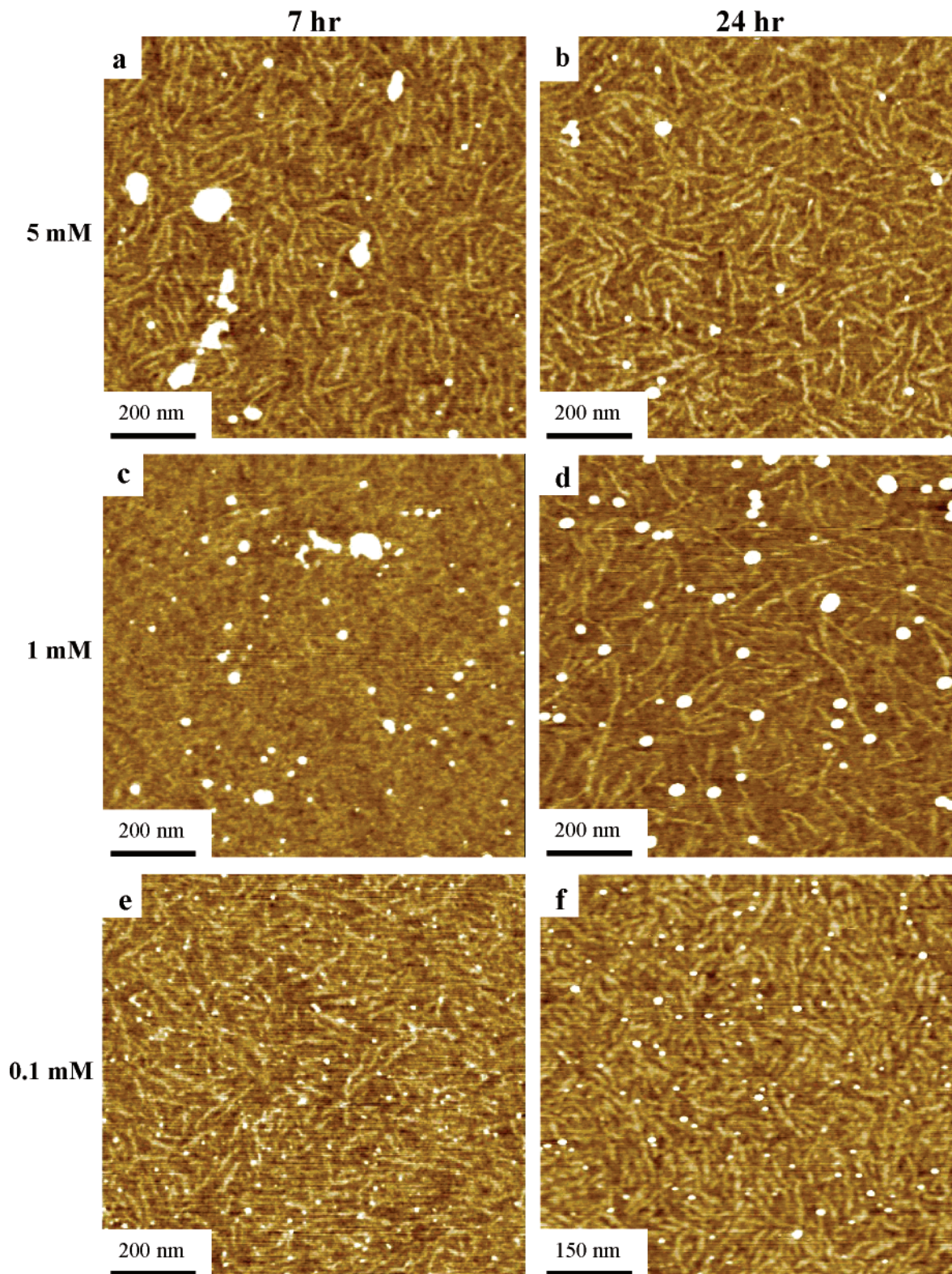


Figure 3. AFM topographical images of HBP–nanoparticle LB monolayers as both time and concentration are varied. The height scale of all images is 10 nm.

diameters was similar to the height distribution determined by AFM (Figure 4b) for a similar experiment, generating a virtually identical diameter of 4.0 nm. This result indicates that the nanoparticles formed from the subphase were in fact true nanospheres with diameters ranging from 2 to 4 nm under most conditions. However, the density of nanoparticles for the identical monolayer was much greater in TEM images than that revealed by AFM, indicating that a significant portion of nanoparticles

was screened by the polymeric monolayer with an effective thickness of 2–4 nm.²⁷

X-ray Scattering Study of Langmuir Monolayers. To gain insight into the formation of silver nanoparticles at the air–liquid interface, X-ray scattering measurements were conducted directly for the Langmuir monolayers. GID studies of the HBP on a subphase of 5 mM AgNO₃ were performed over a period of 12 h while the surface pressure was held constant at 10 mN/m.

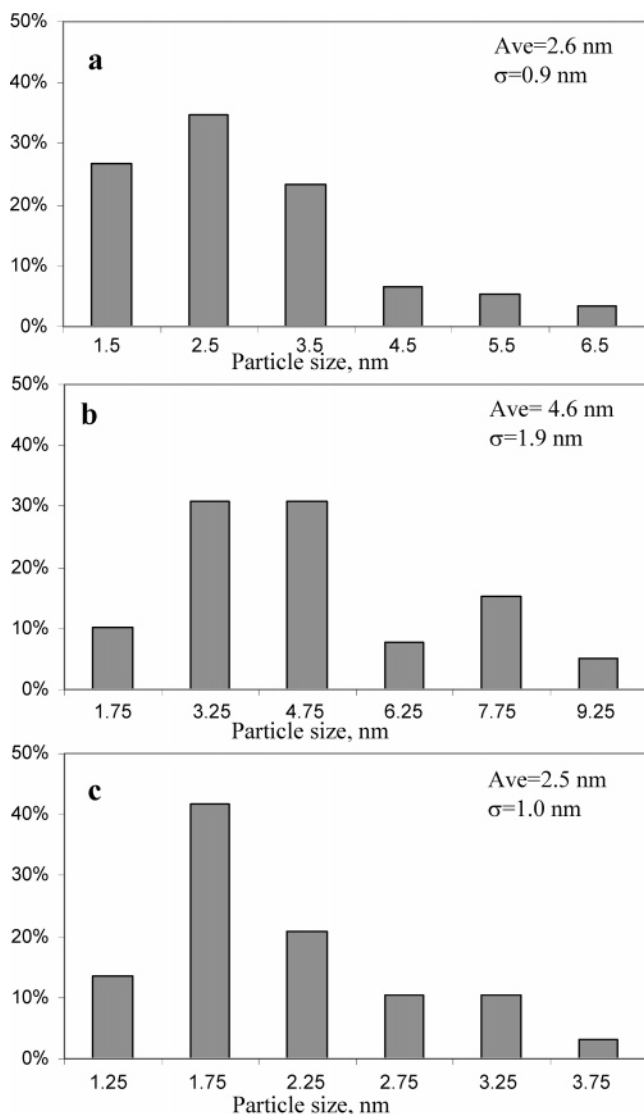


Figure 4. Representative examples of histograms of particle heights observed in AFM images: (a) 1 mM AgNO_3 , 7 h experiment; (b) 0.1 mM AgNO_3 , 7 h experiment; (c) 0.1 mM AgNO_3 , 24 h experiment.

This pressure was targeted because previous studies of the HBP at the air–liquid interface indicated that the HBP’s terminal alkyl tails exhibited ordered hexagonal packing at this pressure.²⁸

After 2.5 h at the AgNO_3 subphase, two diffraction peaks were observed on GIXD scans (Figure 6a). The first peak, at $Q_{xyz} = 14.6 \text{ nm}^{-1}$, was previously shown to correspond to the limited hexagonal ordering and tilting of the HBP’s alkyl tails in the [10] direction of the two-dimensional lattice. However, the correlation length for intramonolayer ordering was less than that observed in previous studies of the HBP on water (5 nm),²⁸ being only 2 nm. This decrease indicates a more disordered state of the alkyl chains in the presence of the silver nanoparticles. The second peak was observed at $Q_{xyz} = 26.5 \text{ nm}^{-1}$. By relating Q_{xyz} to the d spacing, which had a value of 0.240 nm, this peak can be assigned to the (111) reflection, which is the strongest reflection of the fcc unit cell of the silver crystal lattice.³⁹ Limited ordering of the silver lattice was observed because the crystallite size was only 1 nm.

After 5.5 h at the AgNO_3 subphase, a disruption of the hexagonal ordering of the alkyl tails occurred as indicated by the decreased intensity of the (10) peak and the shorter correlation

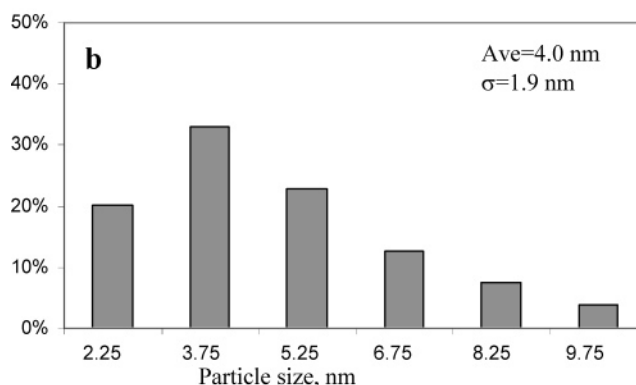
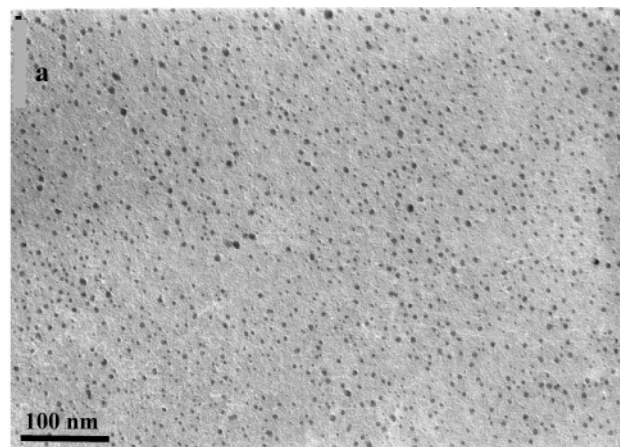


Figure 5. TEM analysis of silver nanoparticles: (a) micrograph of sample fabricated using 0.1 mM AgNO_3 in the subphase for a 7 h period of time (scale bar, 100 nm); (b) particle size distribution histogram calculated from the TEM image.

length (1.7 nm) (Figure 6a). Furthermore, during this same period of time was observed a significant increase in the intensity of the 0.240 nm peak. The (111) peak of the silver crystal lattice was observed to become not only more intense but also refined. The size of the silver particle crystal lattice slightly increased to 1.3 nm, which was close to but lower than the nanoparticle diameter evaluated from AFM data. This difference indicates limited internal long-range order with a significant defect presence that affects X-ray peak broadening. Two new, distinct sharp peaks appeared in the data as well (Figure 6a). These two peaks, occurring at $Q_{xyz} = 19.7$ and 22.4 nm^{-1} , corresponded to d spacings of 0.32 and 0.28, respectively. These peaks are an indication of the directional growth of orthorhombic AgNO_3 crystals beneath the Langmuir monolayer. The reflection planes observed can be assigned to the (210) plane for the peak at $Q_{xyz} = 19.5 \text{ nm}^{-1}$ and to the (113) plane for the peak at $Q_{xyz} = 22.4 \text{ nm}^{-1}$.⁴⁰ The crystallite size in the direction of the (210) peak was 17.3 nm whereas that in the (113) direction reached 15 nm (Table 1). The phenomenon of directional growth of an inorganic phase under an amphiphilic monolayer at the air–liquid interface has been observed before.⁴¹ However, this growth primarily occurred from a supersaturated solution of the inorganic salt. In contrast, the growth and ordering at the air–water interface beneath the HBP monolayer occurred from a dilute solution of AgNO_3 .

(40) JCPDF no. 6-0363, Philadelphia, PA, 1967.

(41) (a) Rajam, S.; Heywood, B. R.; Walker, B. A.; Mann, S.; Davey, R. J.; Birchall, J. *J. Chem. Soc., Faraday Trans* **1991**, *87*, 727. (b) Rapaport, H.; Kuzmenko, I.; Berfeld, M.; Kjaer, K.; Als-Nielsen, J.; Popovitz-Biro, R.; Weissbuch, I.; Lahav, M.; Leiserowitz, L. *J. Phys. Chem. B* **2000**, *104*, 1399. (c) Xu, G.; Yao, N.; Aksay, I. A.; Groves, J. T. *J. Am. Chem. Soc.* **1998**, *120*, 11977. (d) Mann, S.; Heywood, B. R.; Rajam, S.; Birchall, J. D. *Nature* **1988**, *334*, 692.

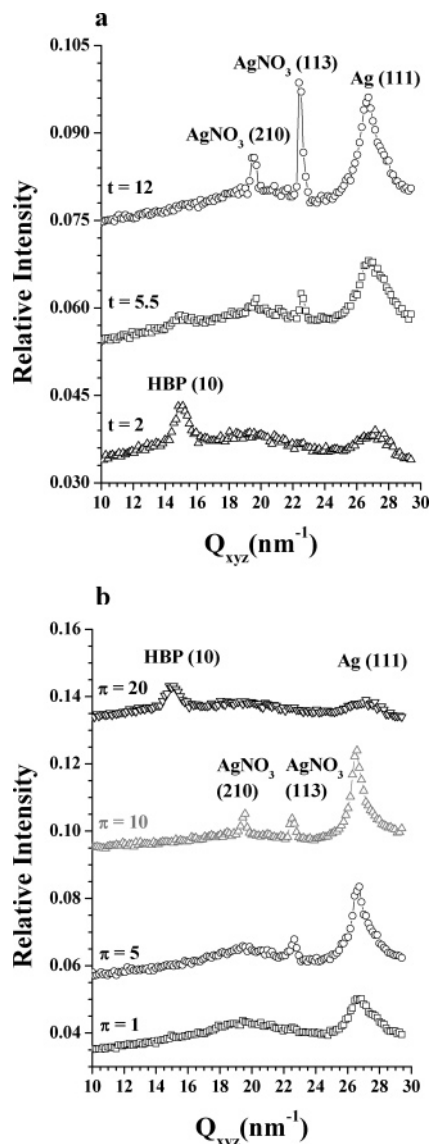


Figure 6. GID data of a Langmuir monolayer on a 5 mM AgNO_3 subphase at different (a) times (hours) and (b) pressures (mN/m). $\beta = 2.25$ for both a and b. Data are offset for clarity.

Finally, at longer times, after 12 h, the HBP alkyl tails situated at the air–monolayer interface became more disordered as indicated by the disappearance of the (10) peak in the X-ray diffraction data. The location of the primary beam was shifted, and the beam was turned off during the waiting period to avoid monolayer damage. Concurrently, the peaks for both AgNO_3 and silver phases became more intense. The crystal lattice size reached 26 nm (evaluation was limited by instrument resolution) in the (210) direction but stayed virtually the same in the (113) direction, indicating strong preferential growth of AgNO_3 crystals in the form of platelets (Table 1). The crystal size of the silver lattice along the (111) direction reached 2 nm, which was still slightly lower than the nanoparticle diameter determined from AFM on the solid support (around 4 nm). In addition, no tracks of large crystals observed with AFM at the solid substrate indicates

that during monolayer deposition only nanoparticles embedded into polymer nanostructures were transferred.

GID measurements were conducted to assess the effects of the surface pressure (density of the surface molecular packing of hyperbranched molecules) on the growth of inorganic crystals at the air–liquid interface. For this experiment, the concentration of AgNO_3 in the subphase remained at 5 mM whereas the specific pressures targeted were 1, 5, 10, and 20 mN/m, which corresponded to different physical states of the monolayers: liquid expanded, liquid, and solid (Figure 2).²⁰ At a surface pressure of 1 mN/m, only the intense diffraction peak from silver nanoparticles ($Q_{xyz} = 26.5 \text{ nm}^{-1}$) was observed with no indication of long-range ordering of alkyl tails as expected for the liquid-expanded state (Figure 6b). The silver crystallite size was 1.5 nm at this pressure, which was comparable to that observed from the previous experiments. At a pressure of 5 mN/m, the silver nanoparticles became larger with a crystal size reaching 2.3 nm. Furthermore, an initial appearance of the AgNO_3 crystals was indicated by characteristic peaks (Figure 6b). The crystallite size in the (113) direction was calculated to be 7.3 nm.

When the surface pressure was increased to 10 mN/m (liquid state of the monolayer with denser packing of alkyl tails), both the $Q_{xyz} = 19.4 \text{ nm}^{-1}$, (210) reflection and the $Q_{xyz} = 22.5 \text{ nm}^{-1}$, (113) reflection were observed, indicating lattice sizes of AgNO_3 crystals of 7.3 and 6.1 nm, respectively (Figure 6b). The crystallite sizes in the (111) direction for silver nanoparticles increased to 3.1 nm. Under these conditions, the alkyl tails were observed to undergo hexagonal packing with limited short-range order.

When the surface pressure was increased to 20 mN/m (solid state of the monolayer with dense intramonolayer packing), the long-range hexagonal ordering of the alkyl tails became clearly visible. The (111) reflection of silver nanoparticles became less refined, exhibiting a correlation length of only 1 nm. This provided the confirmation that the packing of the tails and the ordering of silver nanoparticles were related. Furthermore, the disappearance of the ordering of AgNO_3 also supported the earlier conclusion that both silver nanoparticle formation and AgNO_3 crystal growth were directly controlled by a delicate balance of interfacial interactions such as exposure and surface density of amine and hydroxyl groups of the core and the level of separation of hydrophobic alkyl tails. Only for slightly compressed cores (20% decrease in the surface molecular area) and alkyl tails desorbed from the air–water interface accompanied by the initial formation of nanofibrillar bundles²⁸ is a balance reached for the adsorption and aggregation of silver ions appropriate for silver-phase growth.

Chemical Composition within LB Monolayers. To obtain evidence of silver nanoparticle formation in HBP monolayers transferred to the solid substrate, XPS was utilized. For the analysis, one sample that was known to contain reduced silver in the HBP monolayer known from AFM and one sample that represented the HBP and silver crystals observed in the GIXD experiment were used. In addition, a reference sample of the monolayer formed on a subphase of Nanopure water was prepared and analyzed under identical conditions to test the possibility of the external infusion of ions or light promoting the formation of the silver phase from the contaminants in the LB trough.

The observational energy spectrum for each of the samples, with the binding energy of the orbitals of observed elements

Table 1. GIXD Data for Crystallite Sizes and Correlation Lengths for Different Phases

$Q_{xyz} \text{ (nm}^{-1}\text{)}$	$d \text{ (nm)}$	2 h L (nm)	5.5 h L (nm)	12 h L (nm)	$\pi = 1 \text{ L (nm)}$	$\pi = 5 \text{ L (nm)}$	$\pi = 10 \text{ L (nm)}$	$\pi = 20 \text{ L (nm)}$	direction
14.6	0.43	2	NA	NA	NA	NA	NA	1.2	HBP (10)
19.4	0.32	NA	17.3	14.8	NA	NA	7.3	NA	AgNO_3 (210)
22.4	0.28	NA	25.7	12	NA	7.3	6.1	NA	AgNO_3 (113)
26.5	0.24	1	1.3	2	1.5	2.3	3.1	1	Ag (111)

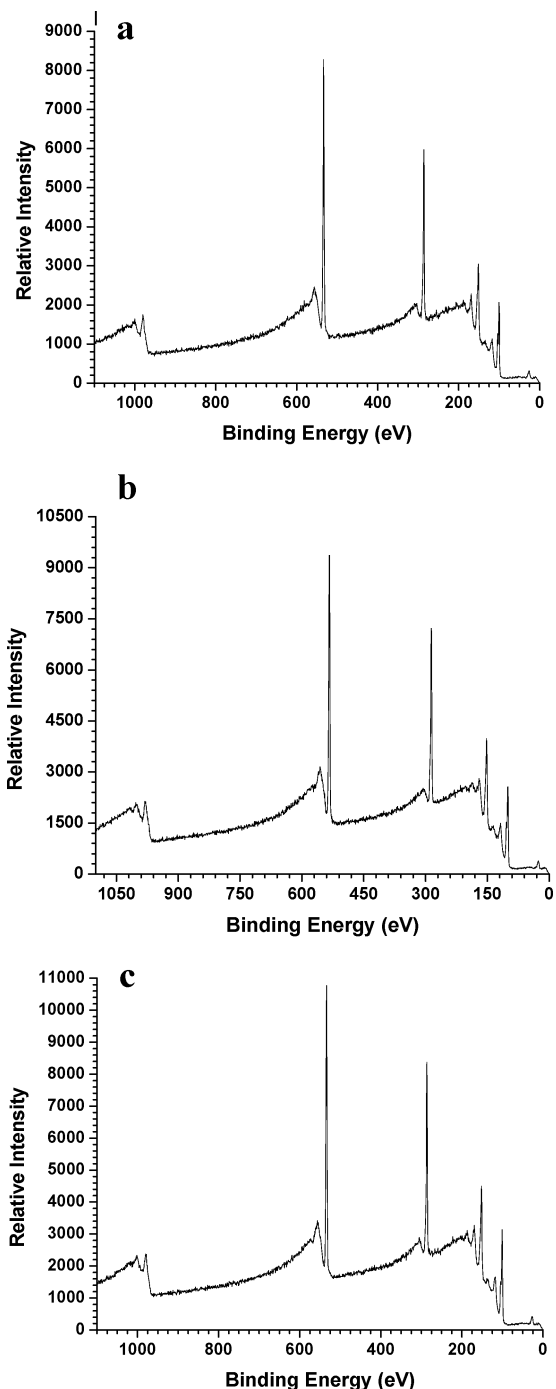


Figure 7. XPS observational energy spectra for LB monolayers (incident angle of 45°): (a) subphase of 5 mM AgNO_3 , reduced after deposition with 1 mM NaBH_4 ; (b) subphase of 5 mM AgNO_3 , no reducing agent used; (c) subphase of H_2O .

indicated, is presented in Figure 7. Silicon, with an Si 2p energy of 99.5 eV,⁴² was used as the reference peak for data analysis because of its abundance in the sample. A high-resolution analysis of the silver binding energy area of the spectrum revealed that elemental silver, with a binding energy of 368.2 eV for the 3d $5/2$ orbital,⁴³ was present in all samples that were fabricated with silver ions in the subphase (Figure 8). The characteristic splitting of the silver 3d peak, with an energy difference of about 6 eV (as reported in the literature⁴⁴), was observed for the silver energy peak in all silver-containing samples studied. The presence of

silver in the sample that was prepared without an additional reduction confirmed the GIXD data in that the growth of silver nanoparticles was occurring at the air–liquid interface. Remarkably, we detected no tracks of silver-related peaks along the peak indicating the presence of the amine groups for the purely polymeric HBP monolayer obtained at the Nanopure water subphase under identical conditions (Figure 8e and f). This is a strong indication that external factors surrounding our experiments at the LB trough cannot contribute to the appearance of the silver phase. Moreover, all of the results from three different surface-sensitive techniques obtained here at three independent troughs were very consistent, thus confirming that the phenomenon observed is related to inherent characteristics of polymer monolayer–metal nanoparticle systems. It is important to note that the data revealed that a peak for AgNO_3 , with a binding energy of 406.6 eV,⁴⁵ did not appear in the analysis for any of the samples in the study (Figure 7). This result indicates that as was suggested from a comparison of X-ray data at the air–water interface and AFM data at solid supports the AgNO_3 crystals were formed in the water subphase and were not transferred to the solid substrate. Thus, it can be certain that the nanoparticles observed with AFM are composed of Ag^0 and not AgNO_3 .

Effect of Electrolyte on Silver Reduction. The modest concentration of silver nanoparticles observed in LB monolayers was not sufficient for us to hypothesize about preferential absorption or templating on hyperbranched molecules. The silver nanoparticles at various subphase concentrations of AgNO_3 appeared to be evenly distributed within the LB monolayer regardless of the clearly visible nanofibril morphology of HBP (Figure 3). Considering that the addition of KCl may promote the absorption of silver colloids in LB monolayers because of the reduced sorption energy barrier, we conducted additional studies.⁴⁶ In this study, KNO_3 was utilized as an electrolyte to ensure more efficient nanoparticle aggregation at the air–liquid interface.

In fact, AFM images of LB monolayers prepared with the addition of 22 mM KNO_3 to 0.1 and 5 mM AgNO_3 (Figure 9) after 7 h of exposure showed higher concentrations of silver nanoparticles. Moreover, a beadlike aggregation of silver nanoparticles along HBP nanofibrils was clearly observed as well (Figure 9). The longest linear aggregates of nanoparticles were observed to be templated by the HBP monolayer when the subphase was 5 mM AgNO_3 . The nanoparticles actually punctuate the nanofibrils in several places; however, the nanofibrils continued uninterrupted on the opposite sides of the particles. This behavior suggested that the nanoparticles may be embedded in nanofibrils by a chemical complexation between the silver atoms and the terminal NH_2 groups, thus facilitating the hydrogen bonding necessary for nanofibril formation (Figure 10).²⁸

It appears that the microstructure of HBP monolayers also provides the mechanism of size regulation of silver nanoparticles that is somewhat similar to a known model for dendritic molecular nanoreactors.¹⁶ The smaller silver nanoparticles may have formed in the hyperbranched cores surrounded by the alkyl shell, thus constraining their growth and limiting their size (Figure 10). The formation of small nanoparticles in these “trapped” regions would have caused a minimal increase in the limiting cross-sectional area in the π – A isotherm, which was observed. The larger particles, however, could have attained their increased size because of a less-constrained growth surface area at the air–liquid interface between the neighboring nanofibrils and their bundles (Figure 10).

(44) Asami, K. *J. Electron Spectrosc. Relat. Phenom.* **1976**, *9*, 469.

(45) Kumar Kaushik, V. *J. Electron Spectrosc. Relat. Phenom.* **1991**, *56*, 273.

(46) Hu, J.-W.; Han, G.-B.; Ren, B.; Sun, S.-G.; Tian, Z.-Q. *Langmuir* **2004**, *20*, 881.

(42) Nguyen, T. P.; Lefrant, S. *J. Phys. Condens. Matter* **1989**, *1*, 5197.

(43) Parry-Jones, A. C.; Weightman, P.; Andrews, P. T. *J. Phys. C* **1979**, *12*, 1587.

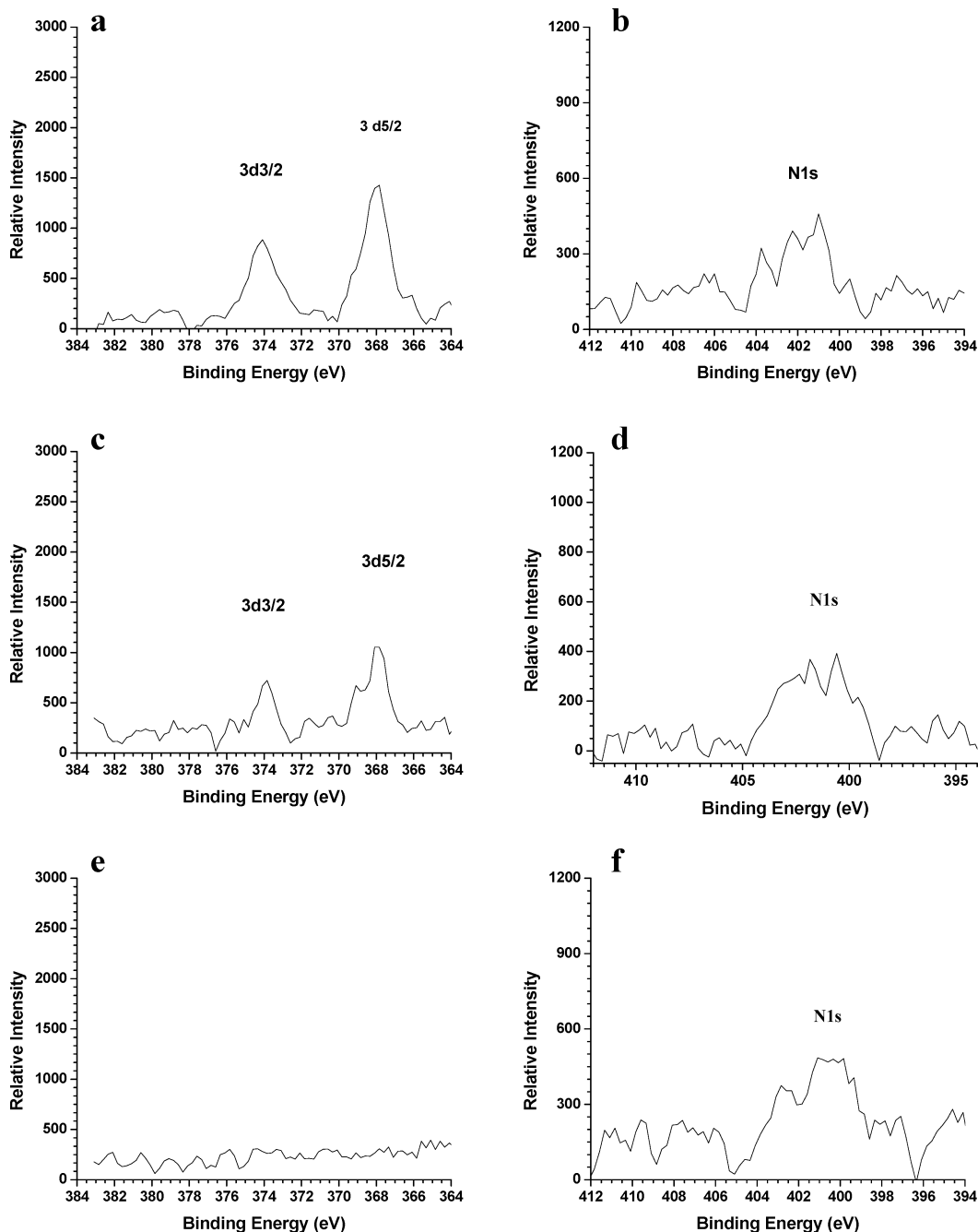


Figure 8. Binding energy spectra of LB monolayers formed on various subphases. (a) Ag 3d: HBP on 5 mM AgNO_3 , reduced after transfer. (b) N 1s: HBP on 5 mM AgNO_3 , reduced after transfer. (c) Ag 3d: HBP on 5 mM AgNO_3 , no reduction agent used. (d) N 1s: HBP on 5 mM AgNO_3 , no reduction agent used. (e) Ag 3d: HBP on water. (f) N 1s: HBP on H_2O .

Post-Transfer Treatments. The templating ability of the nanofibril morphology was further tested using aqueous 1 mM NaBH_4 as a reducing agent after LB transfer. The chemical structure of HBP is stable in the presence of NaBH_4 (a known mild reducing agent often used for the reducing synthesis of nanoparticles), and it did not react with HBP. This technique was chosen to reduce any ions that might have been present in the monolayer after transfer. The LB monolayer was deposited as usual after 7 h of exposure to 5 mM AgNO_3 as a subphase onto the silicon substrate. After that, the sample was dipped into a reducing solution, quickly rinsed with NanoPure water to remove any excess reducing agent, and dried under nitrogen. Using this treatment, a higher concentration of small nanoparticles having an average height of 2.6 ± 0.6 nm was obtained (Figure 11a). Often nanoparticles form long chainlike groups stretching over 100 nm.

However, the nanofibril morphology of the HBP appeared to have been completely disordered by rinsing in solutions. Furthermore, the increased density of nanoparticles indicated that a large number of silver ions and their clusters were present in the monolayer “hidden” under the topmost layer of alkyl tails as suggested in the sketch of the monolayer–silver microstructure (Figure 10). However, if a large number of nanoparticles had formed between adjacent HBP molecules under the canopy of alkyl tails, then the rearrangement of the alkyl tails after treatment with NaBH_4 would have caused them to become more visible in light AFM scanning, which is sensitive mainly to the topmost surface layer. Moreover, a careful analysis of the dimensions of these nanoparticles performed with a calibrated AFM tip shape revealed that the width of the nanoparticles was significantly larger than their heights. Thus, we concluded that these nanoparticles were predominantly *platelets* or *disks* lying parallel

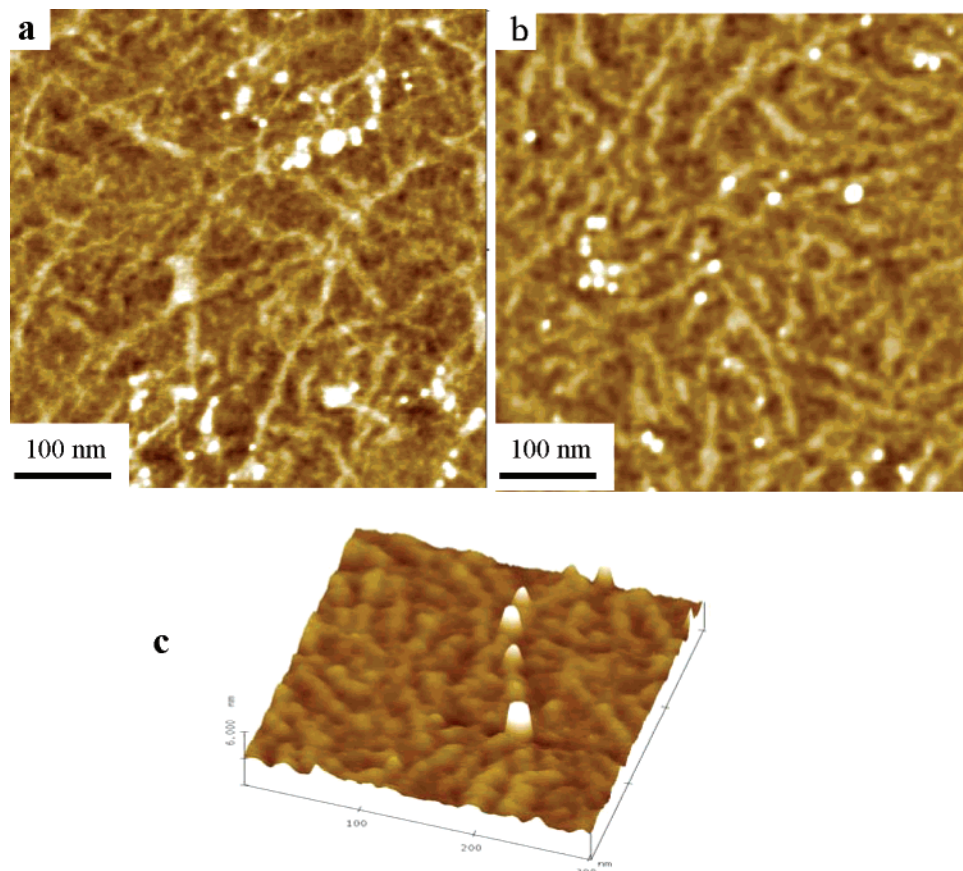


Figure 9. AFM topographical images for LB monolayers obtained with the addition of 22 mM KNO_3 to (a) 5 mM AgNO_3 subphase, 7 h (z scale is 10 nm); (b) 0.1 mM AgNO_3 subphase, 7 h experiment (z scale is 8 nm); (c) 3-D AFM image showing how particles follow nanofibrils.

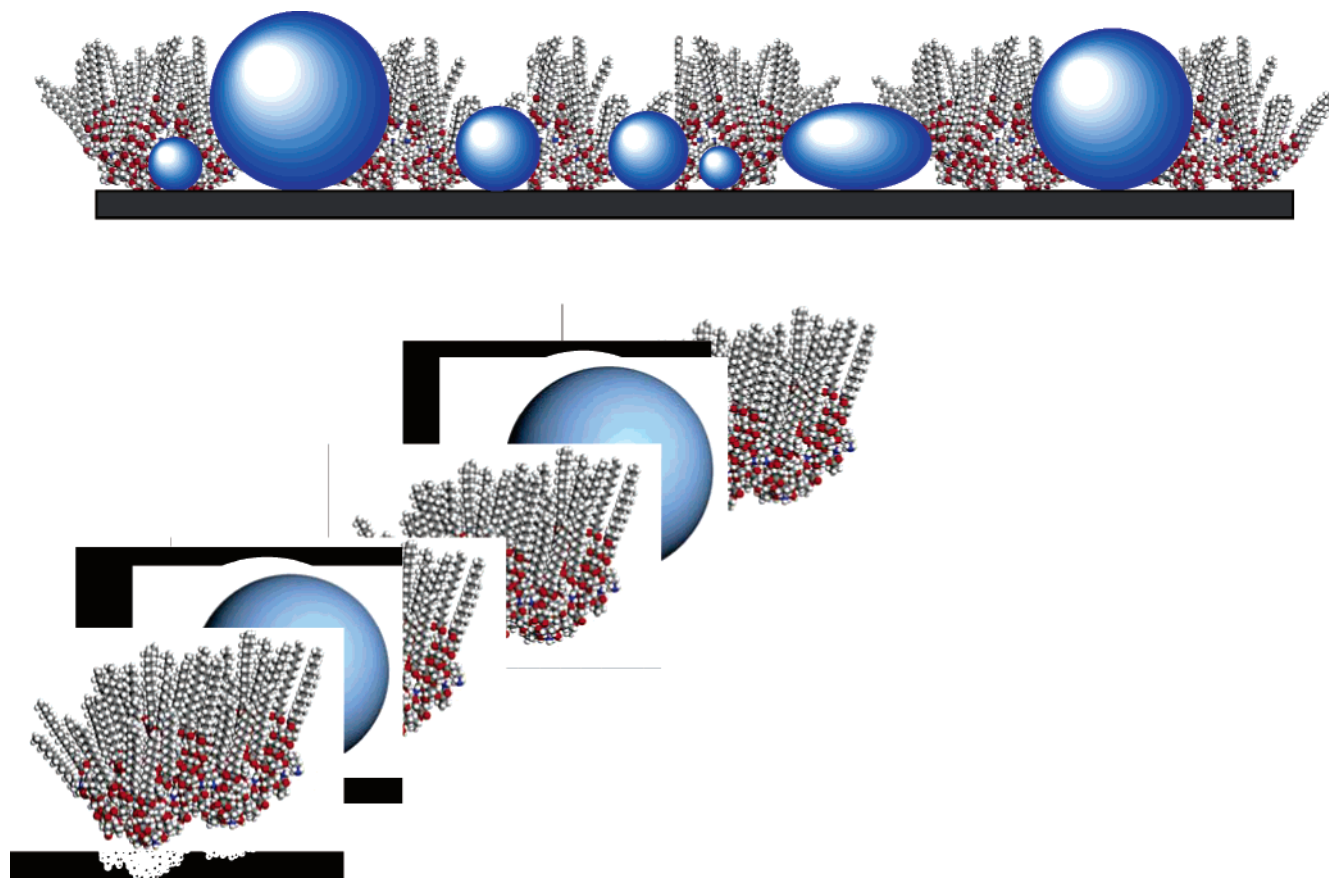


Figure 10. (Top) Cartoon suggesting several different ways the nanoparticles may be templated by the molecular structures: small-diameter nanoparticles trapped inside the amine-hydroxyl cores, large particles suited between micelles, and discoid nanoparticles exposed at disordered regions. (Bottom) Nanoparticle arrangement along the individual nanofibril.

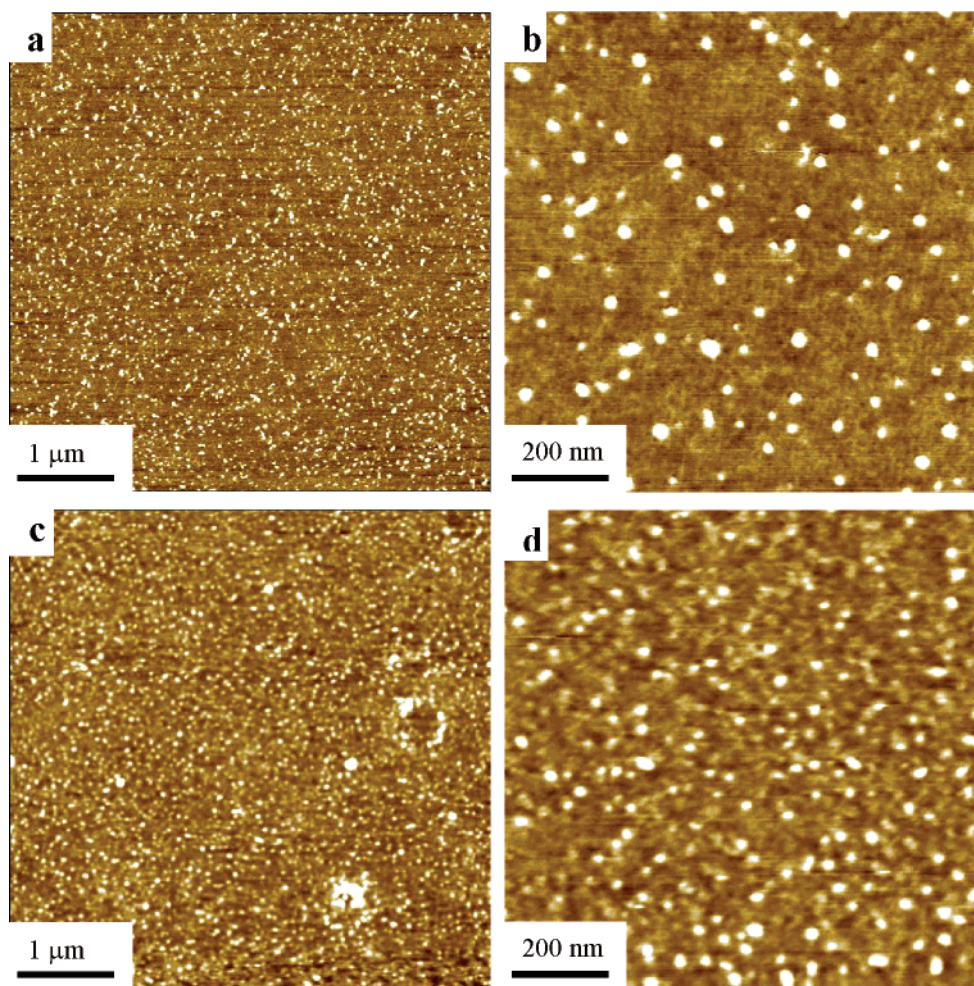


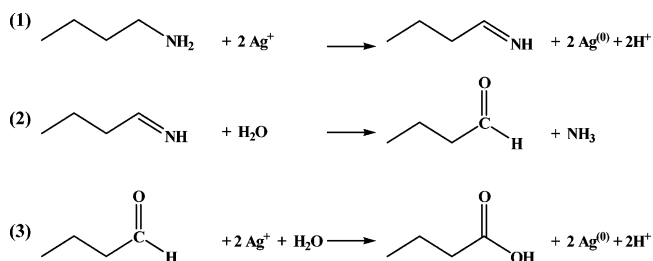
Figure 11. AFM images showing the surface morphology of LB monolayers transferred from a high-concentration subphase (5 mM AgNO_3) after postdeposition treatment: (a, b) rinsed with NaBH_4 ; (c, d) rinsed with H_2O . The height scale is 10 nm.

to the solid surface as suggested in a cartoon in Figure 10. Moreover, similar treatment with Nanopure water that completely disrupts the nanofibrillar morphology revealed a number of anisodiametric nanoparticles as well (Figure 11).

Nanoparticle Formation Mechanism. As known, amine chemical groups are hardly ever used as reducing agents for metal nanoparticle synthesis because of the weak reducing ability afforded by most amines.⁴⁷ However, in this study we observe that primary amine groups of the hyperbranched polymer provided not only ligation for silver ions on multiple metal coordinating sites but also reducing potential for silver nanoparticle formation.

Unlike synthetic polymers, metal-catalyzed amine oxidation is widespread in biology, reflecting a diverse role for amine compounds in nature.^{48,49} The local increase in the concentration of silver ions in amine group-catalyzed amine oxidation has been shown previously.⁵⁰ It was theorized that the silver underwent a cyclic process of reduction and oxidation due to the other oxidizing species present in the reaction. The coordination number of a silver atom, 4, would allow for a tetrahedral coordination complex to form between neighboring silver ions and/or amine

Scheme 1. Redox Reaction for the Formation of Metallic Silver



groups. Mechanism of oxidation of terminal amine-group induced by the localized increase in silver concentration is presented in (1) of Scheme 1. The reaction products are two metal silver atoms and the oxidation of the amine to an imine. Next, spontaneous hydrolysis of the unstable imine group occurs. The oxidation product is ammonia (NH_3) and an aldehyde (step 2). Step 3 presents the well-known oxidation of an aldehyde to carboxylic acid by ionic silver. This reaction is known as Tollen's reaction in carbohydrate chemistry, and it has been used for the silvering of mirrors.⁵¹ In this step, silver complexes with ammonia to form $\text{Ag}(\text{NH}_3)^+$, which can be reduced by the aldehyde group.

Therefore, for each terminal-amino site, the generation of four reduced silver atoms participating in the formation of silver nanoparticles might result. Thus, a single hyperbranched molecule

(47) Stadtman, E. R. *Annu. Rev. Biochem.* **1993**, *62*, 797.

(48) (a) Ouellette, A. J. A.; Anderson, L. B.; Barry, B. A. *Proc. Natl. Acad. Sci. U.S.A.* **1998**, *95*, 2204. (b) Roberts, J. L., Jr.; Sugimoto, H.; Barrette, W. C., Jr.; Sawyer, D. T. *J. Am. Chem. Soc.* **1985**, *107*, 4556.

(49) (a) Kramer, R. M.; Li C.; Carter, D. C.; Stone, M. O.; Naik, R. R. *J. Am. Chem. Soc.* **2004**, *126*, 13282. (b) Naik, R. R.; Stringer, S. J.; Agarwal, G.; Jones, S. E.; Stone, M. O. *Nat. Mater.* **2002**, *1*, 169.

(50) (a) Bacon, R. G. R.; Stewart, D. J. *Chem. Soc. C* **1966**, 1384. (b) Bacon, R. G. R.; Hanna, W. J. W.; Stewart, D. J. *Chem. Soc. C* **1966**, 1388. (c) Bacon, R. G. R.; Hanna, W. J. W. *J. Chem. Soc.* **1965**, 4962.

(51) Jiang, H.; Manolache, S.; Wong, A. C. L.; Denes, F. S. *J. Appl. Polym. Sci.* **2004**, *93*, 1411.

with a core containing 13 to 14 amine groups can reduce up to 64 silver atoms, which can occupy a volume with an effective size of 1 nm. Presented experimental results indicate that the amine-terminated cores of at least three adjacent molecules should participate in the formation of a single nanoparticle.

Conclusions

In conclusion, we demonstrated how hyperbranched amphiphilic copolymer that is capable of self-assembling into nanofibrillar structures in LB monolayers can be developed into a macromolecular scaffold for the synthesis of silver nanoparticles. Spontaneous silver reduction in LB monolayers from these molecules gives monolayers of small nanoparticles, 2–4 nm in diameter, with a narrow distribution of diameters. We suggest that the coupled constraints of the air–liquid interface and the unique morphology of the multifunctional hyperbranched polymer controlled the growth of silver nanoparticles with dimensions of 2–4 nm. The overall size of the silver nanoparticles was controlled and did not exceed the size of the spread hydrophilic core exposed to the monolayer–water interface (3 to 4 nm).

Silver nanoparticle formation reported here was suggested to occur via the mechanism of oxidation of primary amine groups

by silver catalysis rarely found for synthetic copolymers. This mechanism is facilitated by the “caging” of silver ions within the localized surface areas dominated by the amine-terminated cores along the nanofibril structures. The reduction routine observed here provides an example of a one-step process in which hyperbranched molecules with alkyl tails desorbed from the monolayer–water interface and slightly compressed amine-hydroxyl cores directly mediated the formation of stable nanoparticles, which are placed along/among/beneath the semi-cylindrical micelles.

Acknowledgment. We kindly thank Mr. Laab for technical support with TEM and Mr. Anderegg for technical support with XPS. The Midwest Universities Collaborative Access Team (MUCAT) sector at the APS is supported by the U.S. Department of Energy, Basic Energy Sciences through the Ames Laboratory under contract no. W-7405-Eng-82. Use of the Advanced Photon Source was supported by the U.S. Department of Energy, Basic Energy Services, Office of Science under contract no. W-31-109-Eng-38. This work was funded by the NSF-DMR-0308982 project and an AFOSR F496200210205 grant.

LA0525269